Available online at www.sciencedirect.com

SciVerse ScienceDirect

Energy Procedia 24 (2012) 245 – 254

Energy Procedia

DeepWind, 19-20 January 2012, Trondheim, Norway

Upper Ocean Response to Large Wind Farm Effect in the Presence of Surface Gravity Waves

Mostafa Bakhoday Paskyabi*, Ilker Fer

Geophysical Institute, University of Bergen, Allégaten 70, 5007 Bergen, Norway

Abstract

The upper ocean response in the presence of a wind farm is studied numerically, taking into account the effect of surface gravity waves. The farm geometry is a simplified rigid rectangle with characteristic size of L aligned with the wind direction. Assuming a typical wind deficit behind the farm, an analytical 2D U-shaped wake profile is applied to drive the upper ocean circulation. The shallow-water equations are modified to include farm characteristic length, wind-wave and wave-current momentum transfer to study the circulation in the rectangular ocean basin. Solutions of this modified expression as a function of the Rossby deformation radius confirm that the upper ocean response in the vicinity of a farm is strongly related to the wave effects. For the numerical study, the Regional Ocean Modelling System (ROMS) and a wave-modified finite volume technique are used that the wave-modified finite volume technique shows a reasonable agreement with ROMS simulation results. Numerical results for both linear and non-linear wave simulations show the existence of horizontal shear stress gradients related to the fluid motion, wave-induced stress and farm characteristic size. The wind and wave forcing by including wind stress, Stokes drift and wave-induced stress creates symmetrical, range-dependent dipoles in the upper ocean. The dipoles are sensitive to wind stress, wave forcing and L, and have tendency to become asymmetric with time. The near-surface Ekman current is affected significantly, and strong upwelling and downwelling occur. The linear numerical solver results, however, show that the pycnocline depth as a response of upper ocean to the farm becomes weaker after almost one day. Including non-linear term, horizontal diffusion, and bottom friction leads to a decrease in the strength of eddies. But, the amplitude of disturbances in the lee of the farm becomes weaker after almost three days.

Keywords:
Offshore wind farm, surface gravity waves, Ekman current, upwelling, downwelling, Stokes drift, ROMS.

1. Introduction

Renewable energy resources such as solar, thermal, hydro, geothermal, wind and wave are of increasing environmental and economic importance [1]. Ocean is a crucial resource for producing relatively clean energy with a great efficiency from tides, ocean currents, waves and winds. The technology for harvesting energy from the ocean, however, is still not ready to be implemented. Nevertheless, due to the offshore

*Corresponding author
Email addresses: Mostafa.Bakhoday@gfi.uib.no (Mostafa Bakhoday Paskyabi), ilker.fer@gfi.uib.no (Ilker Fer)

1876-6102 © 2012 Published by Elsevier Ltd. Selection and/or peer-review under responsibility of SINTEF Energi AS.
doi:10.1016/j.egypro.2012.06.106

wind technology's achievements in design and application of offshore wind turbines, and public's growing demand for clean and renewable energy, the offshore wind energy has been one of the fastest growing energy source during the last decade. Full scale, operational offshore wind turbine farms need further studies to make them more efficient and cost effective. Environmental and design constraints are needed to support health and management of the nation's marine resources.

Some concern has been expressed about the impact of large scale use of wind power on the local and global meteorology. Likewise, constructing multiple wind farms in the ocean within the same area will likely have negative impacts such as effect of change in temperature on the distributions of clouds and precipitation, effect of electric cables on the fish migrations, influence of sound noise generated by the power plant on the marine communication system, and wind shadowing between wind mills [2]. The magnitude and extent of wind wakes downstream of wind farms are the key parameters that can influence the balance between the negative and positive environmental and economical impacts of the offshore wind power. Wind turbines in a farm influenced by the wake from upstream turbines experience a flow field which is substantially altered compared to an isolated turbine, which in effect reduces power production and increases fatigue loads. Meanwhile, the magnitude of wind wake from a large wind turbine farm and the vertical extent of wind profile behind an operating wind farm influence the upper ocean response to this structure [3]. Ripples, waves, wind gusts, rapid changes in the wind direction and other disturbances in the atmosphere downstream of a wind farm increase the complexity of wake modeling and make it difficult to capture the upper ocean response.

Wind turbines are constructed in regions of strong winds where large surface gravity waves, with great potential of affecting both the upper ocean mixing and wind profile, will also occur. From a physical point of view, the presence of a large obstacle in the ocean will disturb both the wind field (wake), the wave field, and the flow regime to produce perturbations that ultimately must have biological consequences. Thus, in addition to the wind field and the ocean current effects, the surface wave field and its influence on the upper ocean response should also be taken into account. In this study, the main objective is to introduce an appropriate and simple theoretical and numerical frame including the surface gravity wave forcing effects to study the upper ocean response in shallow water regions in the presence of a large wind farm. The study is based on the idealized set up of [3], which considered the wind stress as a forcing mechanism. We modify the two-dimensional shallow water wave equations by including wave stress and Stokes drift to study the wind-driven circulation. For numerical simulation, we implemented a finite volume technique and tested its skill against the Regional Ocean Modelling System (ROMS) [4, 5].

2. Methods

2.1. Spectral wave model

For wave forcing, the Simulating WAves Nearshore (SWAN) model is used [6]. This model solves wind wave generation and propagation in the coastal regions and also includes the diffraction, refraction and shoaling, dissipation due to wave breaking, bottom friction and whitecapping. A general form of the differential equation solved by SWAN in 2D Cartesian coordinates can be expressed as

$$\frac{\partial N}{\partial t} + \frac{\partial c_x N}{\partial x} + \frac{\partial c_y N}{\partial y} + \frac{\partial c_\theta N}{\partial \theta} + \frac{\partial c_\sigma N}{\partial \sigma} = \frac{S_{tot}}{\sigma}, \tag{1}$$

where t denotes time, x and y are the horizontal axes, $c_{x,y}$ are the group velocities in the x- and y-direction, and $c_{\sigma,\theta}$ are propagation speed in frequency domain and directional space, respectively. $N(x, y, \theta, \sigma, t)$ is the action density spectrum, i.e. the ratio of the wave energy spectrum and the relative frequency, σ. S_{tot} is

$$S_{tot} = S_{in} + S_{ds} + S_{nl},$$

where S_{nl} is the non-linear wave-wave interaction term, S_{in} is the wind energy input into the wave field and S_{ds} is the wave dissipation due to whitecapping, breaking and bottom friction.

2.2. Modified shallow water wave

The shallow water wave equations in 2D are described by the water depth $h(x, y, t)$, and two horizontal velocity components $u(x, y, t)$ and $v(x, y, t)$. These equations are derived from the 3D Euler equations for a rotating flow by vertical averaging, and using the hydrostatic pressure assumption. The conservative form of the governing equations can be written as

$$\frac{\partial \Theta}{\partial t} + \frac{\partial \mathbf{F}(\Theta)}{\partial x} + \frac{\partial \mathbf{G}(\Theta)}{\partial y} = \mathbf{S}(t), \tag{2}$$

in which

$$\Theta = \begin{bmatrix} h \\ uh \\ vh \end{bmatrix}, \ \mathbf{F}(\Theta) = \begin{bmatrix} uh \\ u^2h + \frac{1}{2}gh^2 \\ uvh \end{bmatrix}, \ \mathbf{G}(\Theta) = \begin{bmatrix} vh \\ uvh \\ v^2h + \frac{1}{2}gh^2 \end{bmatrix},$$

and the wave-modified external source term $\mathbf{S}(t)$ is given as

$$\mathbf{S}(t) = \frac{1}{\rho_w} \begin{bmatrix} 0 \\ \tau_x - \tau_{in}^x - \tau_B^x \\ \tau_y - \tau_{in}^y - \tau_B^y \end{bmatrix} + \begin{bmatrix} 0 \\ f_{cor}(v + v_s) - \mathbf{F}_{ds}^x \\ -f_{cor}(u + u_s) - \mathbf{F}_{ds}^y \end{bmatrix},$$

where $\mathbf{F}_{ds}$ is the wave-induced momentum transfer from waves to ocean due to dissipation of wave energy, $\vec{\tau}_B$ is the bottom friction velocity vector, f_{cor} is the Coriolis parameter, u_s and v_s are the x and y-components of the Stokes drift, $\mathbf{U}_s$, respectively. Using the wave energy spectrum $E(f, \theta)$,

$$\mathbf{U}_s(z) = 4\pi \int_\theta \int_f f\mathbf{k} E(f, \theta) e^{-2k|z|} df d\theta, \tag{3}$$

where $\mathbf{k}$ is the wavenumber vector, f is the frequency in Hz and θ is the direction in degrees. The contribution to the Stokes drift is maximal in the peak region of the wave spectrum. Meanwhile, near the surface, short waves give a significant contribution to $\mathbf{U}_s$. τ_x and τ_y are the two-components of the total wind stress, and τ_{in}^x and τ_{in}^y are the wave-induced stresses that can be expressed

$$\vec{\tau}_{in} = 2\pi\rho_w \int_f \int_\theta f\widehat{\mathbf{k}} S_{in}(f, \theta) d\theta df. \tag{4}$$

Here, ρ_w is water density and $\mathbf{k} = \widehat{\mathbf{k}}k$ is the horizontal wavenumber vector with modulus k and direction $\widehat{\mathbf{k}} = (\cos\theta, \sin\theta)$.

Assuming a thin layer of fluid with density ρ_0 and thickness h overlying a deep, motionless layer of density ρ_w, ignoring the bottom friction effects and the wave-induced momentum redistribution term, a set of linear partial differential equations are obtained that are identical to the linearized non-linear shallow water equations (2), except that gravity is replaced by the reduced gravity, $g' = g\Delta\rho/\rho_w$. This two-layer approximation is typically applicable for the deep ocean. We apply it for an idealized shallow water study to give a simple analytical explanation. By using some mathematical manipulations based on the above mentioned assumptions, the following expression for active thickness is obtained:

$$\begin{aligned} \frac{\partial}{\partial t}\left[\left(\frac{\partial^2}{\partial t^2} + f_{cor}^2\right) - g'h_0\nabla^2\right]h - f_{cor}^2\nabla.\mathbf{U}_s &= -\frac{f_{cor}}{\rho_w}\left[\nabla \times (\vec{\tau} - \vec{\tau}_{in})\right] \\ &- \frac{\partial}{\partial t}\left[f_{cor}\nabla \times \mathbf{U}_s + \frac{1}{\rho_w}\nabla.\vec{\tau} + \frac{1}{\rho_w}\nabla.\vec{\tau}_{in}\right]. \end{aligned} \tag{5}$$

The stand-point of this part is the ability of the modified shallow water equations as a simple benchmark to show the general response of the ocean to a large wind farm. To this extent, we neglect the impact of

the second-order time derivative, and obtain the following expression by assuming constant wind and wave characteristics

$$\frac{\partial}{\partial t}\left[f_{cor}^2 - g'h_0\nabla^2\right]h = f_{cor}\nabla.\mathbf{U}_s - \frac{f_{cor}}{\rho_w}\nabla\times\vec{\tau} + \frac{f_{cor}}{\rho_w}\nabla\times\vec{\tau}_{in}. \quad (6)$$

Equation (6) is non-dimensionalized by introducing characteristic scales f_{cor}^{-1}, L, and $\Delta\tau(f_{cor}\rho_w L)^{-1}$, for time, length, and the active layer thickness, respectively. Using the same notation and by integrating in time, the non-dimensional form of Eq. (6) becomes

$$\left[1-\gamma^2\nabla^2\right](h-h_0) = -t\nabla\times\left(\frac{\vec{\tau}}{\Delta\tau} - \frac{\vec{\tau}_{in}}{\Delta\tau}\right) + t\frac{\rho_w}{\Delta\tau}\nabla.\mathbf{U}_s, \quad (7)$$

where $\gamma = \sqrt{g'h_0}/(f_{cor}L)$ is the ratio of the Rossby radius of deformation to the length scale. An analytical expression for constant wind and wave forcing is used to model the disturbances behind the wind turbine farm with characteristic length L as

$$\Lambda = \Lambda_{init} - \Delta\Lambda_* P(X,Y) \quad (8)$$

where X and Y shows horizontal axes, $\Lambda = [\vec{\tau}\ \vec{\tau}_{in}\ \mathbf{U}_s]^T$ is forcing vector, $\Delta\Lambda_* = [\Delta\vec{\tau}\ \Delta\vec{\tau}_{in}\ \Delta\mathbf{U}_s]^T$ is the wind and wave forcing fluctuation vector, Λ_{init} is the initial forcing vector, and the function P gives the distribution of forcing behind wind turbine farm as

$$P(X,Y) = \exp\left(-\left(\frac{2Y}{\alpha L+\beta X}\right)^2\right)\max\left(\frac{X\exp((1-X)/L)}{L}, 0\right), \quad (9)$$

where α and β are adjustable variables such that $\alpha+\beta=1$. Here, the choice of P, and $\alpha = 0.8$ and $\beta = 0.2$ is after Broström [3].

2.3. Numerical Approach

To model the shallow water wave equations, we use a wave-modified finite volume technique. Additionally, we use ROMS for comparison. ROMS uses finite-difference approximations on a horizontal curvilinear Arakawa C grid and on a vertical stretched terrain-following coordinate. ROMS provides a flexible structure that allows multiple choices for many of model components such as several options for advection schemes, turbulence models, and lateral boundary conditions. Furthermore, the SWAN wave model is used to generate the wave stress.

2.4. Wave and wind field

SWAN model is not coupled to the modified shallow water wave runs but used only to compare the SWAN result with the analytical representation of wave forcing and wind stress. For this simulation, a monopile is considered in the computational domain as a circular obstacle with 6 m diameter and with its circumference divided into 6 line segments. The reflection coefficient is set to unity to get an upper limit on the reflected wave energy from the monopile. Since no wave should penetrate the impermeable obstacle, the transmission coefficient is set to zero. The computational domain in this setup is 50 m in the x, and 100 m in the y direction. Water depth is 20 m, and the wave frequency range is $[0.04, 0.5]$ Hz.

The results (not shown) show that the shape of wind stress is approximately correlated with the pattern of the wave field for the large directional spreading of the wave energy spectrum. Thus, for the purposes of this study to present the idealized behavior of the upper ocean response, the analytical expression for wind stress and wave parameterizations, Eq. (8) is sufficient. Figure 1 shows the shape of disturbance of x-component of wind stress in the lee side of a large wind farm with characteristic length L. Results are reminiscent of [3]. For the wind speed $\mathbf{U}_{10} = (u_{10}, v_{10})$ at the reference height of 10 m, the wind stress is calculated by $\vec{\tau} = \rho_a C_D \mathbf{U}_{10}|\mathbf{U}_{10}|$ in which $\rho_a = 1.2$ kg m^{-3} is the air-side density and the wind-farm-induced

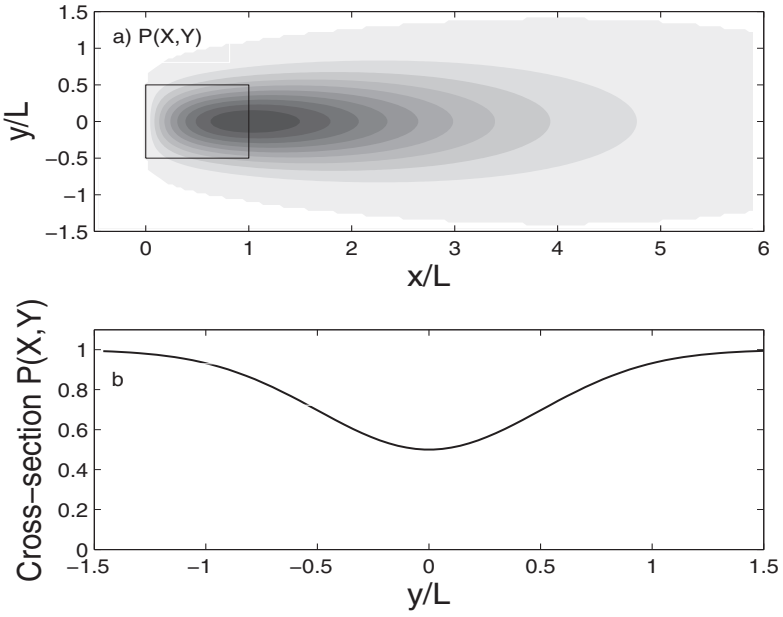

Fig. 1. a) Pattern of wind stress and wave forcing and b) cross-section of the pattern function.

change of the total wind stress is assumed $\Delta\vec{\tau} \approx 0.5\vec{\tau}$. C_D is a drag coefficient dependent on the wind speed.

Computation of wave stress is more complex than that of the wind stress. For convenience, the wave stress defined in Eq. (4) can be separated into two parts

$$\vec{\tau}_{in} = \vec{\tau}_{in}^{L} + \vec{\tau}_{in}^{H},$$

where the first and second terms on the right-hand-side refer to integration of Eq. (4) for intervals $[f_{min}, f_{cut}]$ and $[f_{cut}, f_{\infty}]$, respectively. Because the wave spectrum is not represented by wave model for $f \geq f_{cut}$, the spectrum for this frequency range is assumed to be proportional to f^{-5}, and the wave spectrum is approximated by $E(f,\theta) = (f/f_{cut})^{-5}E(f_{cut},\theta)$ [7]. In the SWAN wave model, the source term S_{in} as a core for calculating the wave stress is parameterized by $S_{in} = 2\pi f(\rho_a/\rho_w)x^2E(f,\theta)$ where $x = \beta_w \max[0, \left(\frac{\mathbf{U}_*^a}{c_p} + z_\alpha\right)\cos(\theta - \theta_{wind})]$ and

$$\beta_w = \frac{1.2}{\kappa^2}\mu \ln^4 \mu, \quad \mu \leq 1,$$

where $z_\alpha = 0.011$ is the dimensionless critical height, $\mathbf{U}_*^a$ is the air-side friction velocity vector, and μ is given by

$$\mu = \frac{gz_e}{c^2}\exp(\kappa/x),$$

Here, $\kappa = 0.41$ the von Kármán constant, and the effective roughness length z_e is expressed as

$$z_e = \frac{z_0}{\sqrt{1 - \frac{\vec{\tau}_{in}}{\vec{\tau}}}},$$

where $z_0 = \alpha[\mathbf{U}_*^a]^2/g$ is the roughness length, $\alpha = 0.009$ is the Charnock's constant. Furthermore, the wind speed profile is given by

$$\mathbf{U}_{10}(z) = \frac{\mathbf{U}_*^a}{\kappa}\ln(\frac{z + z_e - z_0}{z_e}).$$

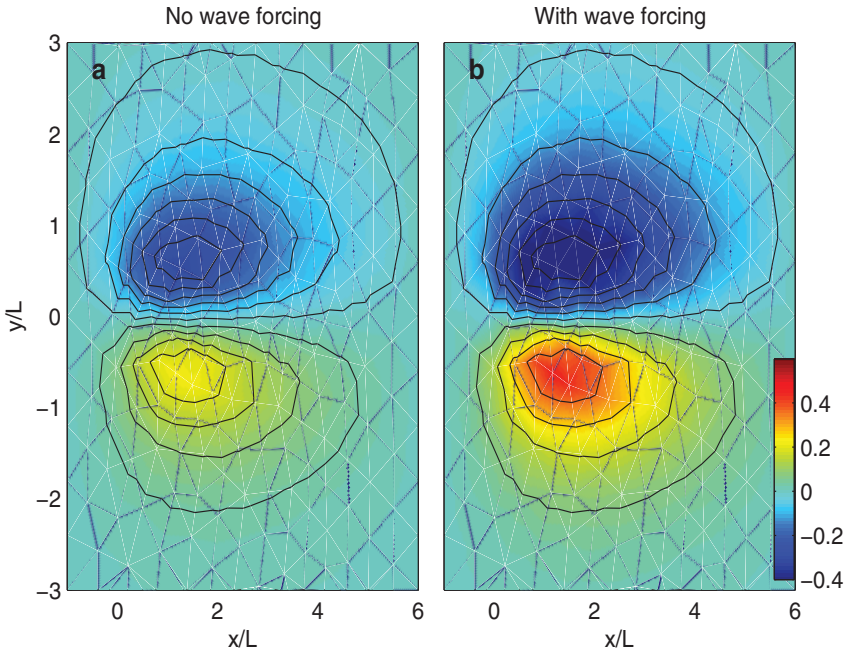

Fig. 2. Non-dimensional thickness of the upper active layer for $\gamma^2 = 1$ for a) no-wave, and b) with wave forcing effect.

3. Results

By calculating S_{in} using above mentioned equations, the wave stress $\vec{\tau}_{in}$ is obtained and the wind-farm-induced change of wave stress is approximated as $\Delta\vec{\tau}_{in} \approx 0.5\vec{\tau}_{in}$. Analog to wind and wave stress, wind-farm-induced change of Stokes drift is given roughly as $\Delta\mathbf{U}_s \approx 4 \times 10^{-3}\mathbf{U}_s$. For the sake of brevity, we did not include the main references of the wave stress calculation and refer to [7] for details. As an example of above mentioned formulations for obtaining vector Λ, its x-component value for wind speed $u_{10} = 10$ and 20 m s^{-1} are $(0.174, 0.0378, 0.119)$ and $(1.01, 0.267, 0.237)$, respectively.

Geophysical flows experience the Coriolis force, due to the Earth's rotation. It is one of the leading terms in the large scale shallow water equations. In this section, we test the skill of two numerical techniques: finite element for simplified model Eq. 7, and a Riemann solver for numerically modelling of linearized form of Eqs. 2 by excluding bottom friction to maintain a linear geostrophic equilibrium, where the Coriolis force is in balance with the elevation gradient. As there is no dissipation, a good numerical scheme should maintain this equilibrium for a long time. The initial active layer thickness is 20 meter. Coriolis parameter f_{cor} is 1.2×10^{-4} s^{-1} in the whole domain. In the numerical experiments of this section, we use a square basin of $20L\times20L$ with $L = 5$ km. For simplicity, bottom frictional effects and non-linear effects are ignored. Figure 2 shows the finite element simulations with and without wave forcing for t=1, $\gamma^2 = 0.54$ and $u_{10} = 10$ m s^{-1} (u_{10} is the x-component of $\mathbf{U}_{10}$). Figure 2-a shows the rising of the pycnocline on the southern side of wind farm and a corresponding depression of the pycnocline due to the geostrophic adjustment on the northern part of farm for no-wave forcing case. However, including wave forcing, especially the Stokes drift, modifies the upper ocean response and leads to a larger amplitude of pycnocline displacement than that in the no-wave case. The spatial response of the upper ocean in terms of the pycnocline depth highly depends on the normalized Rossby deformation radius γ^2. In Fig. 3, the maximum value of the pycnocline depth as a function of γ^2 is shown. It can be seen that the amplitude of upper ocean response to the farm

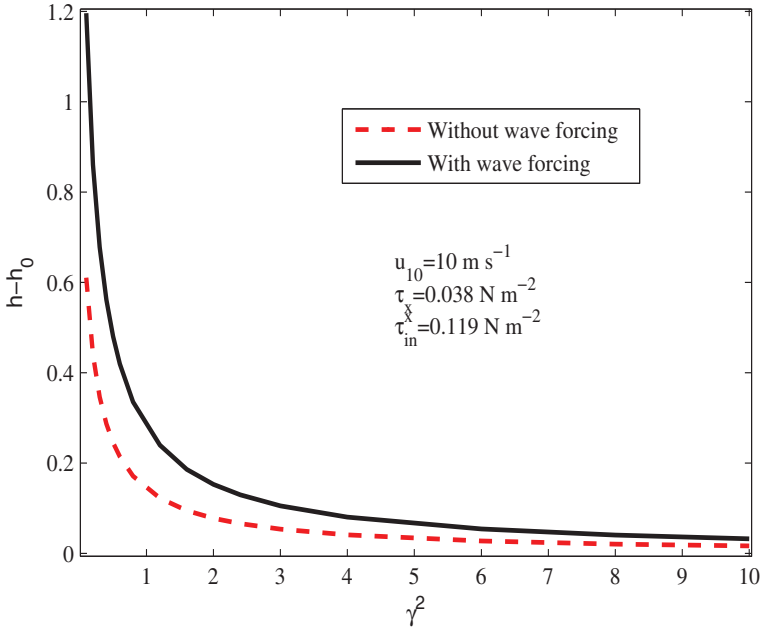

Fig. 3. The maximum amplitude of pycnocline depth as a function of γ^2. The solid line shows the results for the case with wave forcing and the dashed line without wave forcing.

in the presence of wave forcing is larger than that without the wave effect, and the amplitude of maximum pycnocline depth decreases with a greater rate in no-wave case by increasing γ^2.

In the previous example, we ignored some important processes such as internal waves to obtain a simple expression for the active layer thickness. These simplifications lead to a linear variation of pycnocline depth by time, and do not capture all important involved physics.

We use the Lax-Friedrichs technique as a member of finite volume family to compute the numerical approximation of Eq. (2). This method is applied on staggered C-grid and can be written without the external source term based on splitting technique as

$$\Theta_{i,j}^{n+1} = \Theta_{i,j}^{n} - \frac{\Delta t}{\Delta x}\left(\mathbf{F}_{i+\frac{1}{2},j}^{n+\frac{1}{2}} - \mathbf{F}_{i-\frac{1}{2},j}^{n+\frac{1}{2}}\right) - \frac{\Delta t}{\Delta x}\left(\mathbf{G}_{i,j+\frac{1}{2}}^{n+\frac{1}{2}} - \mathbf{G}_{i,j-\frac{1}{2}}^{n+\frac{1}{2}}\right), \tag{10}$$

where

$$\mathbf{F}_{i+\frac{1}{2},j}^{n+\frac{1}{2}} = \frac{\mathbf{F}(\Theta_{i,j}^{n}) + \mathbf{F}(\Theta_{i+1,j}^{n})}{2} - \frac{1}{2}\left|\lambda\left(\frac{\Theta_{i,j}^{n} + \Theta_{i+1,j}^{n}}{2}\right)\right|(\Theta_{i+1,j}^{n} - \Theta_{i,j}^{n}),$$

and $|\lambda|$ denotes the determinant of λ. Analog to above expression, other terms will be updated at each time-step. $\lambda(\Theta)$ is the linear advection speed and can be interpreted as non-linear speed, and for $\mathbf{F}$ and $\mathbf{G}$, it is given as

$$\frac{\partial \mathbf{F}(\Theta)}{\partial \Theta} \text{ and } \frac{\partial \mathbf{G}(\Theta)}{\partial \Theta}.$$

The external source term is imposed to governing equations by the following ordinary differential equation

$$\frac{\partial \Theta}{\partial t} = \mathbf{S}(t).$$

To simulate linear shallow water wave by this technique, we apply analytical representation for wind stress and wave parameterizations by using Eq. (9) for constant wind speed $\mathbf{U}_{10} = (10, 0)$. Figure 4 shows the

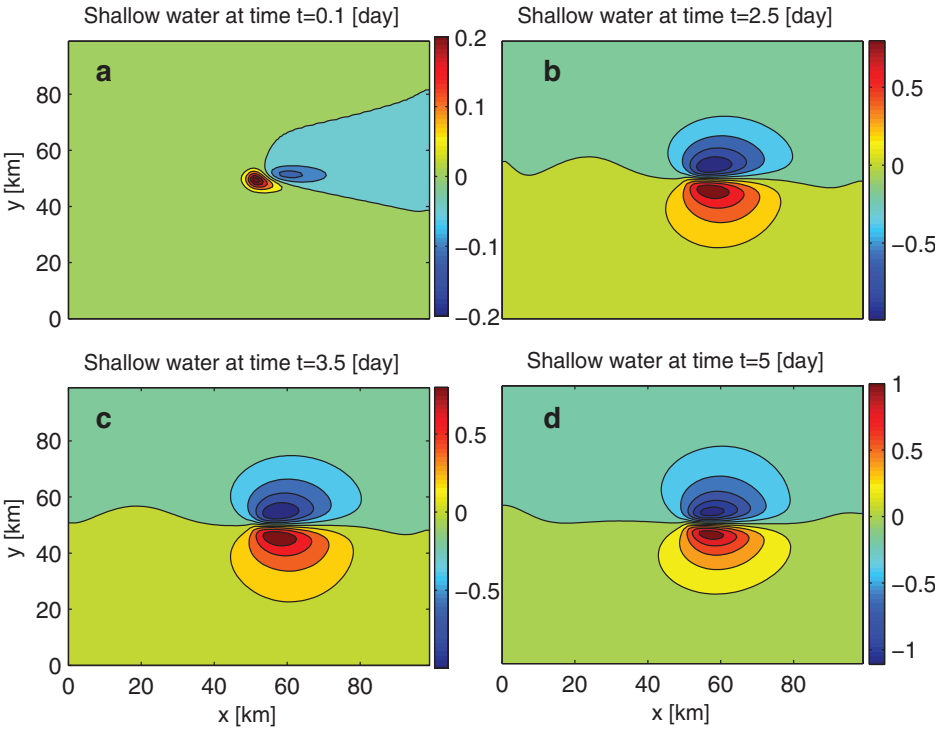

Fig. 4. Results of the Lax-Friedrichs technique for simplified shallow water wave at: a) 0.1 day, b) 2.5 day, c) 3.5 day and d) 5 day. After about 1 day, the upper ocean response to the constant wind and wave forcing becomes weaker. Note the change of scales on the colorbars

generation of two eddies as a result of wind stress and wave forcing on the large wind farm. This figure presents time evolution of pycnocline depth for 5 days. The farm blocks the flow of the winds and wind-generated waves to form extended lee regions downwind. It can be seen that the northern and southern part of the lee regions of farm are locations of Ekman divergence and convergence. Ekman transport takes place in the near surface layer and is to the right of the wind in the northern hemisphere. At the southern region of the lee, upwelling of deeper waters must compensate the divergence, while at the northern region, sinking must occur. The upwelling and downwelling elevate or depress, respectively, the pycnocline from its unperturbed depth.

In the next example, we solve Eq. (2) by using the wave-modified finite volume technique by considering the non-linear momentum advection term, horizontal diffusion term and the bottom friction for 5 days (Fig. 5). Obtained results show much less variation in pycnocline depth. For confirming results, we run the two-dimensional configuration of ROMS model for a duration of about 5 days (Fig. 6). We use periodic boundary conditions for both numerical techniques. Results show reasonable agreement between ROMS simulations and the Lax-Friedrichs solutions. Meanwhile, results show that the ignored terms for obtaining Eq. (7) play a significant role; using linear two-layer shallow water wave can not capture all important features of the problem.

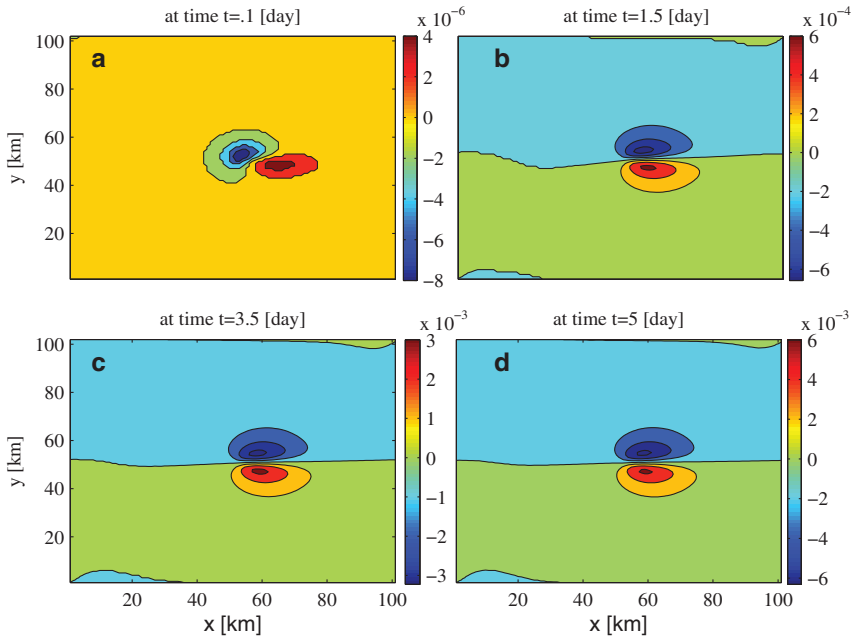

Fig. 5. Results of the Lax-Friedrichs technique for non-linear shallow water wave by including bottom friction, horizontal diffusion term at : a) 0.1 day, b) 2.5 day, c) 3.5 day and d) 5 day. After about 3 day, the upper ocean response to the constant forcing becomes weaker and we see a very slow linear growth in the pycnocline depth.

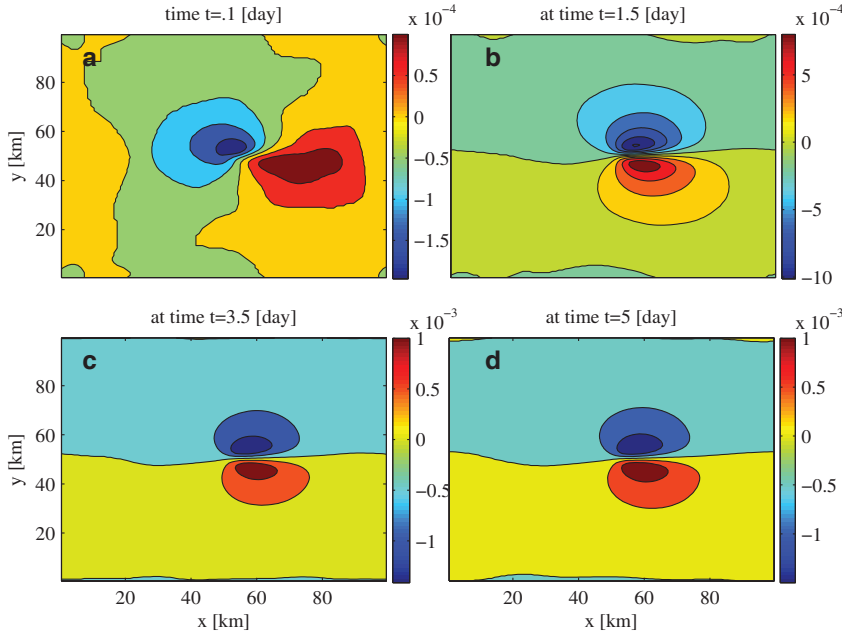

Fig. 6. Spatial disturbances in the pycnocline depth by using the 2D results of ROMS at: a) 0.1 day, b) 2.5 day, c) 3.5 day and d) 5 day.

4. Conclusions

In this study, the upper ocean response in shallow water in the presence of a large offshore wind farm with characteristic length scale L was investigated using two 2D numerical models: a wave-modified finite volume technique based on the Lax-Friedrichs technique, and ROMS. The amplitude of the upper ocean response is found to be strongly sensitive to the wave forcing. Furthermore, when the wave forcing is included, the amplitude of the maximum pycnocline depth for a given Rossby radius is greater than that in the no-wave case. In both cases, the maximum pycnocline depth approaches zero when the normalized Rossby radius approaches infinity. Simulations showed that the winds and wind-driven waves passed a large wind turbine farm generate eddies downstream. The scale of eddies are close to L and their time scale is several days, depending on L. Linear solutions show that the pycnocline depth response of upper ocean becomes weaker after about one day. Including the non-linear term, horizontal diffusion, and bottom friction effect led to a decrease in the strength of the eddies. The amplitude of disturbances in the lee regions of the farm becomes weaker after about three days. This investigation presented a methodology for modifications, and parameterizations of the 2D shallow water wave in order to incorporate the influence of surface wave forcing into an ocean model in the presence of a large wind farm. These modifications and suggested analytical expression for wind and wave field in the numerical models merit further studies.

5. Acknowledgements

This work has been funded by the Norwegian Center for Offshore Wind Energy (NORCOWE) under grant of the Research Council of Norway.

References

[1] J. Twidell, T. Weir, Renewable energy resources, Taylor and Francis, 2009.
[2] C. Wang, R. Prinn, Potential climatic impacts and reliability of very large scale wind farms, Tech. rep., MIT Joint Program on the Science and Policy of Global Change, No. 175 (2009).
[3] G. Broström, On the influence of large wind farms on the upper ocean circulation, J. Mar. Syst. 74 (2008) 585–591.
[4] A. F. Shchepetkin, J. McWilliam, The regional ocean modeling system: a split-explicit, free-surface, topography-following coordinates ocean model, Ocean Modell. 9 (2005) 347–404.
[5] J. Kämpf, Advanced Ocean Modelling:Using Open-Source Software, Springer-Verlag, 2010.
[6] N. Booij, R. Ris, L. Holthuijsen, A third-generation wave model for coastal regions. Part I : Model description and validation., J. Geophys. Res. 104 (1999) 7649–7666.
[7] M. Bakhoday-Paskyabi, I. Fer, A. D. Jenkins, Surface gravity wave effects on the upper ocean boundary layer: modification of a one-dimensional vertical mixing model, Cont. Shelf Res. accepted.